Robotica (2019) volume 37, pp. 2056–2072. © Cambridge University Press 2018
doi:10.1017/S0263574718001340

A Novel Generation of Ergonomic Upper-Limb Wearable Robots: Design Challenges and Solutions

Giorgia Ercolini†*, Emilio Trigili†, Andrea Baldoni†, Simona Crea†‡ and Nicola Vitiello†‡

† *The BioRobotics Institute, Scuola Superiore Sant'Anna, Pisa, Italy*
E-mails: e.trigili@santannapisa.it, a.baldoni@santannapisa.it, s.crea@santannapisa.it, n.vitiello@santannapisa.it
‡ *IRCCS Fondazione Don Carlo Gnocchi, Milan, Italy*

(Accepted November 25, 2018. First published online: December 26, 2018)

SUMMARY
In this work we present NEUROExos, a novel generation of upper-limb exoskeletons developed in recent years at The BioRobotics Institute of Scuola Superiore Sant'Anna (Italy). Specifically, we present our attempts to progressively (i) improve the ergonomics and safety, (ii) reduce the encumbrance and weight, and (iii) develop more intuitive human–robot cognitive interfaces. Our latest prototype, described here for the first time, extends the field of application to assistance in activities of daily living, thanks to its compact and portable design. The experimental studies carried out on these devices are summarized, and a perspective on future developments is presented.

KEYWORDS: Exoskeletons; Control of robotic systems; Mechatronic systems; Neurorehabilitation; Series elastic actuators.

1. Introduction

Robotic rehabilitation was proposed in the early 1990s as a tool for providing intensive and repetitive treatments to promote the recovery of the motor functions and movement coordination compromised by neurological disorders.[1] After a stroke, improving arm function is a core element of the rehabilitation, with the final goal of enabling the patient to recover motor functions and perform activities of daily living (ADL) independently.[2]

Compared to traditional physical therapy, rehabilitation robotics hold the potential to reduce the physical effort required of the therapist (enabling him/her to treat more than one patient at a time), to provide more objective and precise measurements of the patient's performance and progress, to adapt to different users' individual needs and abilities, and to maintain a high level of patient engagement.[3]

Robotic devices for upper-limb rehabilitation can be classified into two main categories according to their mechanical structure: end effector robots and exoskeletons. End effectors are characterized by a single interaction point with the patient (typically the hand or the forearm), which holds the arm and generates forces to guide or resist the movement. This connection makes the device easily adaptable to a wide range of patient anatomies and clinical conditions, but on the other hand, the lack of a tight coupling between the robot and the user can lead to undesirable forces and uncomfortable positions of the human arm. Examples of end effector devices are the MIT-MANUS,[4] which allows passive and active mobilization of the wrist and elbow in the horizontal plane, the GENTLE/s,[5] a

Giorgia Ercolini and Emilio Trigili have contributed equally to this work.

* Corresponding author. E-mail: giorgiaercolini7@gmail.com

https://doi.org/10.1017/S0263574718001340 Published online by Cambridge University Press

cable-driven system for gravity compensation, and the MIME,[6] which allows guidance of the paretic limb by the unimpaired one.

On the other hand, exoskeletons allow more accurate control of human movement, as they are able to control forces and/or positions of each joint independently. Exoskeletons are designed to operate in parallel with human limbs, reproducing the physiological kinematics during functional movements. Given the close physical human–robot interface (pHRI), the design of an exoskeleton has to comply with strict requirements for appropriate safety and ergonomics, in order to guarantee a smooth and comfortable interaction between the user and the device.[7] *An ergonomic exoskeleton* is a system that does not introduce constraints (i.e. it is "transparent") to the user's movement. This transparency involves both actuation and kinematic aspects.

Kinematic transparency refers to the device's compatibility with the kinematics of the user's joints. Indeed, a fundamental feature of the pHRI is its capability to achieve and maintain alignment between the actuated joint axis and the functional rotation axis of the corresponding human joint. When designing an exoskeleton, it is paramount to consider the laxity of biological joints, whose axes are not fixed (i.e. they can translate or rotate) during the execution of a movement. Joint axis misalignments can be the cause of reaction forces between the robotic frame and the human joints or body segments, which can generate pressure at the interface, causing discomfort or irritation, especially in cases of patients with skin-sensitivity problems. To optimize the human–robot kinematic coupling, it has typically been proposed to integrate passive degrees of freedom (pDoFs) to preserve the alignment between human and robot rotational axes.[8]

Actuation transparency refers to the capability of the control system to provide zero impedance (i.e. zero torque) during movement, leaving the user free to move without receiving assistive or resistive forces. This control scheme is typically referred as *transparent mode*.[9] On top of the transparent mode, the so-called *assistive strategy* of a wearable robot can be designed to provide an action, for example, to assist, resist, or perturb the movement, depending on the rehabilitation exercise. To implement the transparent mode of the robot, impedance or admittance control strategies can often be designed to "virtually" modify the output joint impedance of the system. In addition to zero-impedance and assistive controllers, gravity compensation mechanisms or algorithms can positively affect the working area of the hemiparetic arm and facilitate the rehabilitation process.[10,11] The weight support of both the arm and the robot represents another fundamental design requirement. This property can be achieved through hardware or software strategies. For instance, the LIMPACT[12] partially or fully sustains the weight of the arm through a structure made of two parallelogram linkages; the DAMPACE[13] provides a gravity compensation force through three independent spring mechanisms placed at the base of the exoskeleton and connected to the elbow and wrist with a cable system. Finally, the HARMONY[14] and the ALEX[15] compensate their own weight and the weight of the user's arm by means of control strategies, without any additional mechanical component.

In order to safely treat the impaired arm, the pHRI should be intrinsically compliant, to protect the arm from excessive loads and to avoid harming the user in case of sudden or resistive movements, such as those due to muscle spasms. A *compliant human–robot interface* can be realized through different approaches, either by incorporating a compliant element into the joint or by implementing a control strategy that virtually simulates the behavior of a compliant interaction.[16] One of the most common solutions to realize compliant actuation units in wearable robotics consists of Series Elastic Actuators (SEAs): in SEAs, an elastically compliant element is placed between the gear train and the output load, with the goal of reducing the overall output impedance of the motor. In accordance with Pratt and Williamson,[17] this type of actuation can be preferred with respect to traditionally stiff motors and rigid linkages, due to its ability to mimic the biomechanical behavior of the body. Specifically, SEA architectures provide the possibility of energy storage (similar to the tendons and other connective tissues), improved fidelity of torque control, increased back-drivability, and shock tolerance.

Another solution to the compliance problem of wearable robots is provided by pneumatic actuators. These motors can absorb undesirable forces through their intrinsic compliance, due to the compressibility of their energy source (air), thus assuring a high force-to-weight ratio and low weight and inertia.[18] Pneumatic actuators can be classified as either (i) pneumatic motors, which provide linear or rotational movement through compressed air, or (ii) pneumatic artificial muscles, consisting of a closed flexible membrane that contracts and extends depending on the fluid pressure inside the chamber. Among such devices, the PNEU-WREX[19] promotes shoulder and elbow rehabilitation through five pneumatic cylinders, whereas RUPERT[20] treats the shoulder, elbow, and wrist

https://doi.org/10.1017/S0263574718001340 Published online by Cambridge University Press

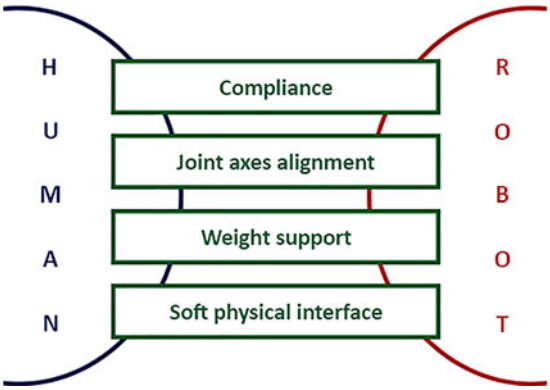


Fig. 1. Human–exoskeleton interface main requirements.

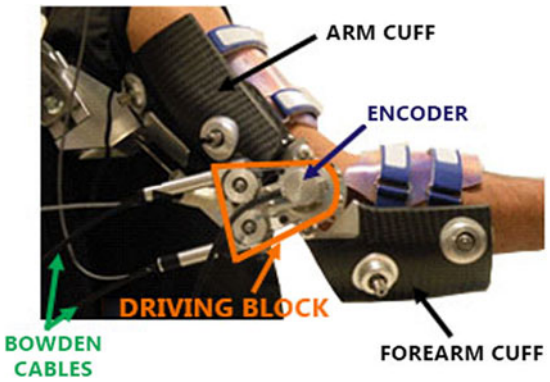


Fig. 2. Overview of NEUROExos Elbow Module v1. © [2018] IEEE. Reprinted, with permission, from ref. [23].

through four McKibben pneumatic muscles, each consisting of a rubber inner tube covered by a helical-wave braid.

In order to optimize the coupling with body segments, the pHRI has to be *soft, comfortable, and able to evenly distribute the pressures over wide contact areas.* Examples of "soft" interfaces are lightweight, custom-made carbon fiber braces combined with comfortable Velcro straps that envelope the arm in the LIMPACT;[12] and rigid half-cylindrical structure combined with an inflatable Velcro strap, similar to a blood pressure cuff, that wraps the arm and forearm in the MEDARM.[10] Similar designs are adopted by "soft" exosuits, that is, powered clothing-like frames coupled with the user through padded arm wraps with Velcro bands,[21] or via buckled neoprene arm enclosures, which allow adjustments to different user anthropometries, preventing tissue slippage and increasing the transmission efficiency.[22]

In consideration of all the aforementioned requirements, summarized in Fig. 1, we have developed several generations of upper-limb wearable robots over the last few years. The following sections provide an overview of the iterative development of successive upper-limb exoskeleton prototypes, emphasizing the progressive fulfillment of system requirements. The ultimate goals of this line of research and development are to deliver effective rehabilitation therapy and to move toward a fully wearable robotic upper-limb system capable of providing assistance in ADL. Novelty with respect to the state of the art is highlighted for each successive prototype.

2. Materials and Methods

2.1. The first generation: NEUROExos Elbow Module v1

The first prototype developed at The BioRobotics Institute is an active orthosis for the flexion and extension of the right elbow, namely the NEUROExos Elbow Module[23] (NEEM v1, shown in Fig. 2). The main novelties introduced by this device are a 4-DoF passive self-alignment mechanism, a remote muscle-like actuation, and a comfortable physical human–machine interface.

https://doi.org/10.1017/S0263574718001340 Published online by Cambridge University Press

The kinematic compatibility between the user and the robot is guaranteed by a passive mechanism that follows the physiological displacement of the elbow axis during movement. The mechanism is realized through a closed chain of 13 passive joints, resulting in a 4-DoF passive mechanism that allows the rotation of the flexion–extension axis in the frontal and horizontal plane, as well as the translation of the forearm link along the flexion–extension axis and in the horizontal plane. As a result, the robot axis can trace a double conic frustum similarly to the human elbow articulation, which results unloaded from undesired translational forces.

The actuation system is realized through a pair of remote and independent antagonistic units, each composed of a nonlinear elastic element; a linear hydraulic actuator with a stroke of 50 mm, controlled by a three-land-four-way proportional electronic valve, powered by a three-phase 1.1 kW AC motor; a stroke amplifier; and a steel-wire rope that transmits the force to the driving block, to which is wrapped around through Bowden cables. The driving block is composed by: a custom-made planetary gear that amplifies the torque by a factor of four, thus helping to reduce the force transmitted by the wire ropes and consequently to reduce friction losses given by the Bowden cables; a frame hosting two force sensors and two mechanical end stops. The latter limits the range of motion to 130° and ensures safety by preventing elbow hyper-extension and hyper-flexion. The sensory apparatus contains a 1024 ppr incremental optical encoder to measure the flexion–extension rotation angle, two custom-load cells to measure the force transmitted by the antagonist tendon cables, and two linear potentiometers to measure the pistons position.

Both the arm and forearm links have a double-shell structure, providing high wearability to fit users with different arm sizes. The external one has a carbon fiber structure that provides structural stiffness, and low encumbrance and weight; the internal one is made of two half shells of polypropylene, covered by a layer of ethylene vinyl acetate, for moisture draining and skin transpiration, coupled with the dorsal and ventral sides of the limb segment. Four elastic elements with a high longitudinal compression stiffness (100 N/mm) link together the external cuff and the internal dorsal one, allowing the transmission of the interaction force between them with small relative motions, thanks to the lower shear stiffness (15 N/mm). The double-shell structure and driving block encompass the user's arm only on the posterior and lateral side, facilitating the donning procedure in case of patients exhibiting muscle hypertonia (i.e. an increase of muscle tone that causes an abnormal arm posture), as of post-stroke patients with elbow spasticity.

The NEEM v1 control algorithms run on a real-time control system (NI PXI-8196 RT, Austin, TX, USA), equipped with a data acquisition card (NI M-series, Austin, TX, USA). The control system has a hierarchical architecture including two main blocks: the high-level layer running at 100 Hz that implements a finite-state machine for the execution of rehabilitation exercises, and the low-level layer running at 1 kHz that, taking the information from the high level, generates the input for actuating the joint, implementing the closed-loop position and force controllers. The outputs of the load cells and the linear potentiometers are sampled at 250 kHz, then low-pass filtered, and down-sampled to 1 kHz.

The compliant actuation is achieved through the combination of hardware and software components, and allows to adjust actively the stiffness of the joint through two different modalities: the passive-compliance and the torque control modes (Fig. 3a).

The passive-compliance controller receives as inputs the desired joint stiffness and the desired joint position and provides the desired piston positions. These are controlled by two independent proportional-integrative (PI) closed-loop regulators that send the desired speeds of the hydraulic pistons to the electronic valves in order to move the joint. This control modality simulates musculoskeletal behavior, generating a convergent force field around the equilibrium position of the limb to attract the human joint to the desired trajectory, allowing deviations that decrease with increasing stiffness.

The torque controller takes as inputs the preload force applied to the antagonist cables and the desired joint torque, to calculate the desired cable forces, controlled by the action of two independent proportional-integrative-derivative (PID) closed-loop regulators. The outputs of the PID regulators are the speed of the hydraulic pistons, controlled by means of the electronic valves. In this case, the exoskeleton can transfer a minimal load to the human arm during active movements of the user. The low output impedance assured by this antagonistic nonlinear elastic actuation is fundamental in case of high frequency disturbance, like spasmodic events, avoiding high and painful interaction forces.

This control system permits to cover a wide range of possible therapeutic interventions, implementing a passive-compliance strategy, in which the robot moves passively the arm of the user along

https://doi.org/10.1017/S0263574718001340 Published online by Cambridge University Press

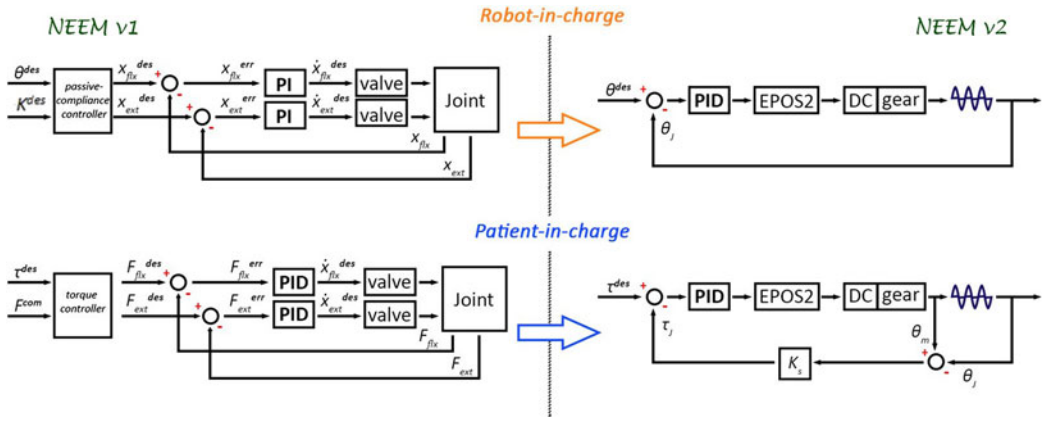


Fig. 3. Evolution of robot-in-charge and patient-in-charge modalities implementation: (a) NEEM v1; (b) NEEM v2 and following versions.

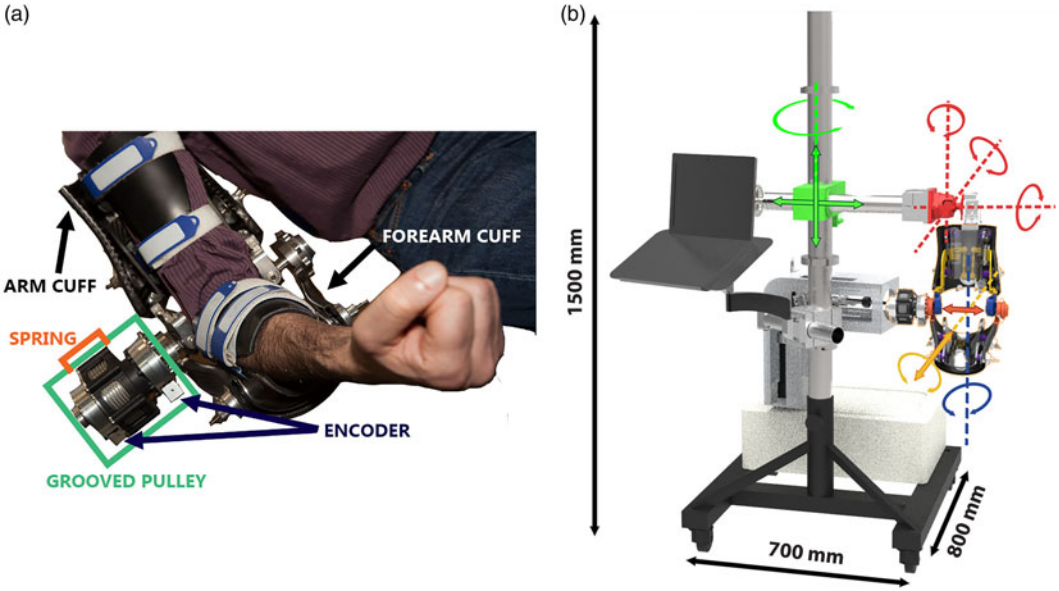


Fig. 4. Overview of the NEUROExos Elbow Module v2: (a) picture of the exoskeleton worn by a subject © [2018] IEEE. Reprinted, with permission, from ref. [24]; (b) CAD model with regulations, passive degrees of freedom and encumbrance.

a desired angular trajectory (*robot-in-charge* mode) and a torque modality which provides a certain level of assistance to complete the task, with an assist-as-needed paradigm (*patient-in-charge* mode).

2.2. NEUROExos Elbow Module v2

In order to improve the joint compliance and usability within clinical settings, the exoskeleton described in the previous paragraph has been revised. The new version (namely NEEM v2,[24] shown in Fig. 4) integrates a new remote actuation unit consisting of: a DC servomotor; a reduction stage (gear ratio 1:80); a grooved pulley with steel cables; a safety clutch that disengages the output shaft and the pulley, in case of excessive torques. The mechanical power is transmitted from the remote actuation unit to the exoskeleton through a pair of Bowden cables. The driving pulley is mounted on the external lateral side of the actuated joint and transmits the motor torque to the elbow shaft through a custom-made torsional spring (stiffness = 98 N·m/rad) enclosed into the pulley assembly. The whole assembly corresponds to a SEA configuration and contains the new sensory apparatus, composed of two 32-bit absolute encoders placed at both extremities of the spring; this intrinsically compliant architecture allows to manage sudden and resistive movements, which are very common in post-stroke subjects affected by elbow spasticity.

https://doi.org/10.1017/S0263574718001340 Published online by Cambridge University Press

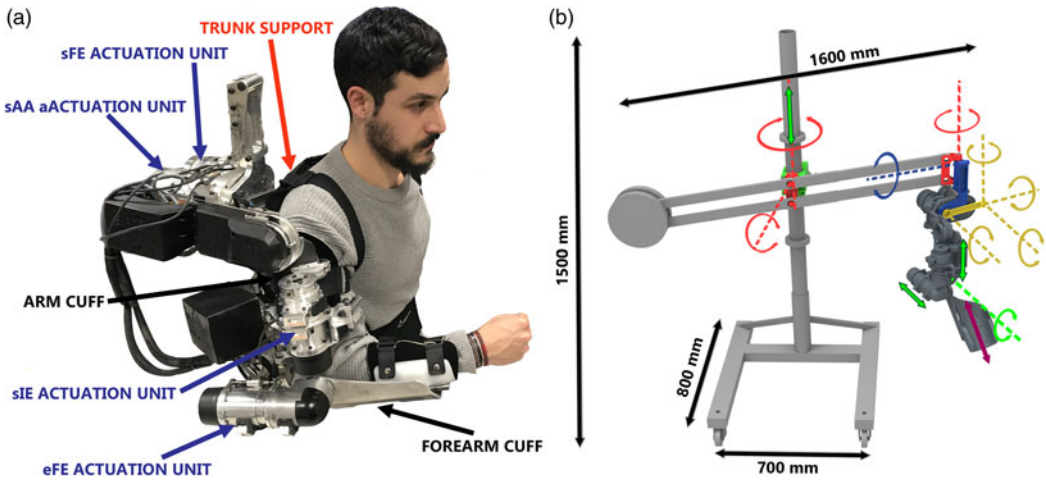


Fig. 5. Overview of NEUROExos Shoulder–Elbow Module-alpha: (a) picture of the exoskeleton worn by a subject; (b) CAD model with regulations, passive degrees of freedom and encumbrance.

The second substantial modification from the previous version was the design of a movable support structure, with embedded regulations to adjust the height and orientation of the device. A movable stand improves the usability of the device in clinical settings, allowing the robot to be easily installed and moved within clinical facilities. The support structure consists of a wheeled platform (700 mm × 800 mm) with a vertical stand (height: 1500 mm), hosting the electronics and actuation unit. As shown in Fig. 4b, the exoskeleton is connected by means of a spherical joint to a bar, embedded in the support structure, which can translate horizontally and vertically and rotate around a vertical axis; these regulations allow the exoskeleton to be adapted to both bedridden and seated users. In this configuration, the user has to sustain only the weight of the forearm structure, reducing the need for a gravity compensation.

A plastic box contains the control electronics, that is, the sbRIO-9632, (National Instruments, Austin, TX, USA), which is featured with both an ARM processor and an FPGA. The ARM controller runs the high-level layers of the control algorithms, while the FPGA runs the low-level controllers. The electronics box also contains the current servo amplifiers and a custom PCB to route the wires from/to the motor unit and sensors.

Similarly to the previous version, NEEM v2 provides both robot-in-charge and patient-in-charge treatment modalities (Fig. 3b). In *joint position control*, a reference angular value is sent as input to the PID controller with the joint angle measured by the encoder placed on the joint side. The output voltage, sent to the driver, allows to bring the joint to the desired position. In *joint torque control*, a reference value of torque is sent to the PID controller with the measured torque, calculated from the spring deflection as the difference between the two encoder values, multiplied for the spring stiffness value. The output current, sent to the driver, allows to provide the desired torque to the joint. When the reference value is set to 0, the user's arm is completely free to move (i.e. *transparent mode*).

2.3. The second generation: NEUROExos Shoulder–Elbow Module-alpha

The NEUROExos Shoulder–Elbow Module-alpha[25] (NESM α, shown in Fig. 5) is an active orthosis for the mobilization of the right shoulder and elbow and consists of a serial kinematic chain with four active and several passive DoFs, connected to a vertical stand on a wheeled platform through an articulated parallelogram, functioning as the weight-relief system and as support for some of the passive DoFs. The platform also hosts the electronics and the control box. As can be seen in Fig. 5b, size regulations are included in the device to fit different anthropometries, in particular for: adjusting the exoskeleton height; rotating and tilting the device upwards; adjusting the axis of rotation of the elbow away from the sagittal plane of the arm; adjusting the orientation of the forearm cuff; regulating the length of the arm.

The double-shell structure of the forearm and arm links of the previous versions is maintained, with an external rigid carbon-fiber structure with aluminum inserts and an internal ergonomic cuff, made by polyethylene coated with a layer of polyurethane foam, attached to the dorsal side of the arm.

https://doi.org/10.1017/S0263574718001340 Published online by Cambridge University Press

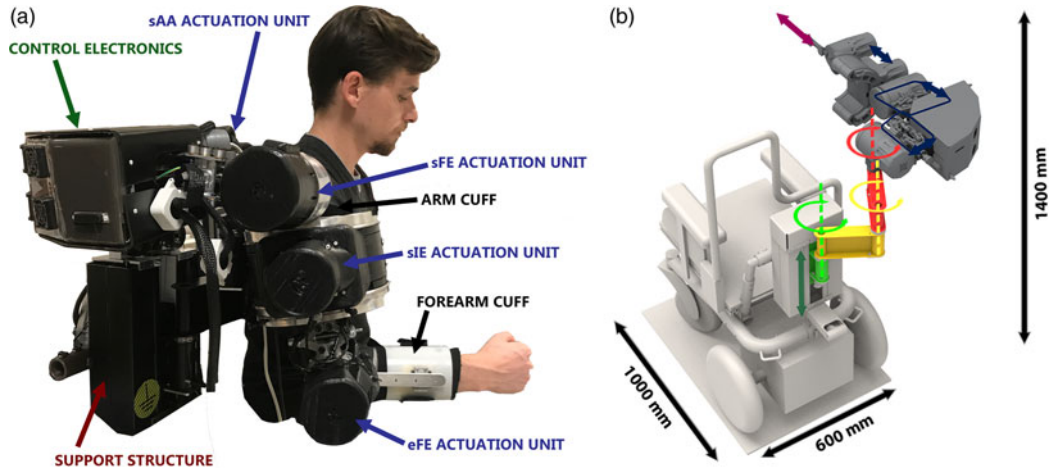


Fig. 6. Overview of NEUROExos Shoulder–Elbow Module-beta: (a) picture of the exoskeleton worn by a subject; (b) CAD model with regulations, passive degrees of freedom, and encumbrance.

The problem of misalignment between human and robot rotational axes has been tackled through the inclusion of different passive DoFs, in particular:

- A slider between the forearm outer and inner cuff represents a simplified mechanism with respect to the NEEM configuration, to allow the elbow rotation axis to move in the backward/forward direction during its flexion/extension movement. Only this passive DoF has been integrated into the elbow joint since it addresses the predominant elbow displacement,[26] while reducing the complexity of the system with respect to the 4-DoF mechanism of the NEEM.
- Three passive DoFs are embedded in the articulated parallelogram. The first DoF allows the shoulder elevation/depression by the motion of the parallelogram along a circular path in its plane, which can be approximated to a vertical translation; similarly, the second DoF allows the exoskeleton movement along a circular path around a vertical-axis rotational joint at the center of the parallelogram, to follow the shoulder protraction/retraction movement. Finally, the exoskeleton is directly attached to a vertical-axis rotational joint, placed at one end of the parallelogram, which allows to compensate for the movement of the torso.
- Four passive DoFs, included in the link connecting the exoskeleton to the trunk support, allow the vertical movement of the scapula during the abduction/adduction movement.

The active DoFs are all rotational joints and allow the elbow flexion/extension (eF/E), the shoulder abduction/adduction (sA/A), flexion/extension (sF/E) and internal/external rotation (sI/E). The sA/A and eF/E actuators are placed in proximity of their anatomical joints, with a rigid transmission; the sI/E and sF/E motions are transmitted through steel cables and pulleys. All actuation units are realized with a SEA architecture, including: a DC servomotor; a reduction stage (gear ratio 1:160 for sA/A and sF/E; and 1:120 for sI/E and eF/E); a custom spring (stiffness of 166 N·m/rad for sA/A and sF/E, and 92 N·m/rad for sI/E and eF/E); two absolute encoders located at the two extremities of the spring; a servo driver.

The control system runs on a real-time controller, a sbRIO-9636 (National Instruments, Austin, Texas, US), endowed with a 400-MHz processor and an FPGA. The high-level layer runs at 100 Hz, while the low-level closed-loop controllers run at 1 kHz. The low-level control implements the joint position and the joint torque modalities similarly to the NEEM v2, as shown in Fig. 3b. In the latter modality, the weight of the exoskeleton can be supported through a gravity compensation algorithm, described in Section 3.3.

2.4. NESM-beta

NESM β, shown in Fig. 6, is a shoulder–elbow exoskeleton developed to overcome the limitations of the α-version. It maintains the SEA architecture and the soft interface with the human arm, but its design was aimed at expanding the usage scenarios. The device can be attached to an electric wheelchair in order to make it portable and potentially assist or rehabilitate in daily-life scenarios

https://doi.org/10.1017/S0263574718001340 Published online by Cambridge University Press

(e.g. in a home environment). Moreover, a flipping mechanism for each joint allows to change easily the arm configuration and mobilize either the left or the right arm, enlarging the end users' population.

The support structure is a metallic box containing a weight relief system, composed of a vertical linear guide where the counterweights, attached to a cable and pulleys stage, can move. The box can be fixed on the rear side of a wheelchair through clutches. The exoskeleton assures high wearability and adaptation to different anthropometric sizes through three jack regulations, each equipped with a potentiometer (maximum stroke = 30 mm). One jack is connected to the sA/A unit and adjusts the relative shoulder rotational axis along the medio-lateral direction; one is attached to the sF/E unit and serves for the translation of the shoulder rotational axis along the anteroposterior direction; the last one is connected to the eF/E joint and is used to regulate the arm length. The forearm and arm links maintain the double-shell structure similarly to the α-version.

In order to match the kinematics of the human arm, the following passive DoFs are included in the device:

- The connection between the exoskeleton and the support structure is realized through a kinematic chain of three rotational joints with vertical axes, connected by two links. This system allows the translation of the exoskeleton shoulder axis in the horizontal plane to follow the shoulder protraction/retraction movement, as well as a rotation around a vertical axis to follow the trunk movements.
- The system of counterweights and pulleys inside the support structure enables the vertical translation of the base of the exoskeleton. This mechanism allows to comply with the shoulder elevation/depression movement.
- A slider placed between the internal and external forearm cuff allows the displacement of the elbow rotation axis in the backward/forward direction, as in the α-version.

It is worth noticing that, with respect to the α-version, the same passive movements of the shoulder center of rotation have been addressed, but in a more compact structure. As shown in Fig. 6b the whole structure lateral encumbrance has been reduced from 1600 mm of the α-version to 600 mm.

The SEA architecture is maintained: sA/A and sF/E actuation units are composed of a DC brushless motor, a 1:160 reduction stage, two 20-bit absolute encoders, a servo-driver, and three custom torsional springs arranged in series. Similarly, sI/E and eF/E actuation units contain a DC brushless motor, a 1:100 reduction stage, two 19-bit absolute encoders, a servo-driver and a single custom torsional spring. Unlike the previous version, the actuation unit for the shoulder flexion/extension is placed in proximity of the anatomical joint axis, substituting the cable transmission with a rigid transmission chain. The actuation unit for the shoulder internal/external rotation is located on the outer lateral side of the exoskeleton, with its rotational axis perpendicular to the joint rotational axis. Motion is transmitted by a gear mechanism that allows the relative rotation between two semi-cylindrical supports (one fixed, the other moving together with the actuator), without invading the space between them.

The control electronics is embedded in the exoskeleton structure, saving room for the power supply box, placed below the seat of the wheelchair. The same control strategies for the patient-in-charge and robot-in-charge modalities of the previous version have been implemented (Fig. 3b).

Moreover, the gravity compensation algorithm developed for this device allows switching the arm configuration (i.e. left or right) without turning off the device.

3. Results and Discussions

The experimental characterizations and studies carried out on the different devices that highlight how the main requirements have been accomplished are collected and described in the following paragraphs.

3.1. Wearability and comfort

The effectiveness of the 4-DoF passive mechanism in aligning the robot and elbow rotation axes has been assessed on NEEM v1. The characterization was conducted using a motion capture system (VICON 460, Oxford, UK) with passive optical markers, with five healthy subjects wearing the

https://doi.org/10.1017/S0263574718001340 Published online by Cambridge University Press

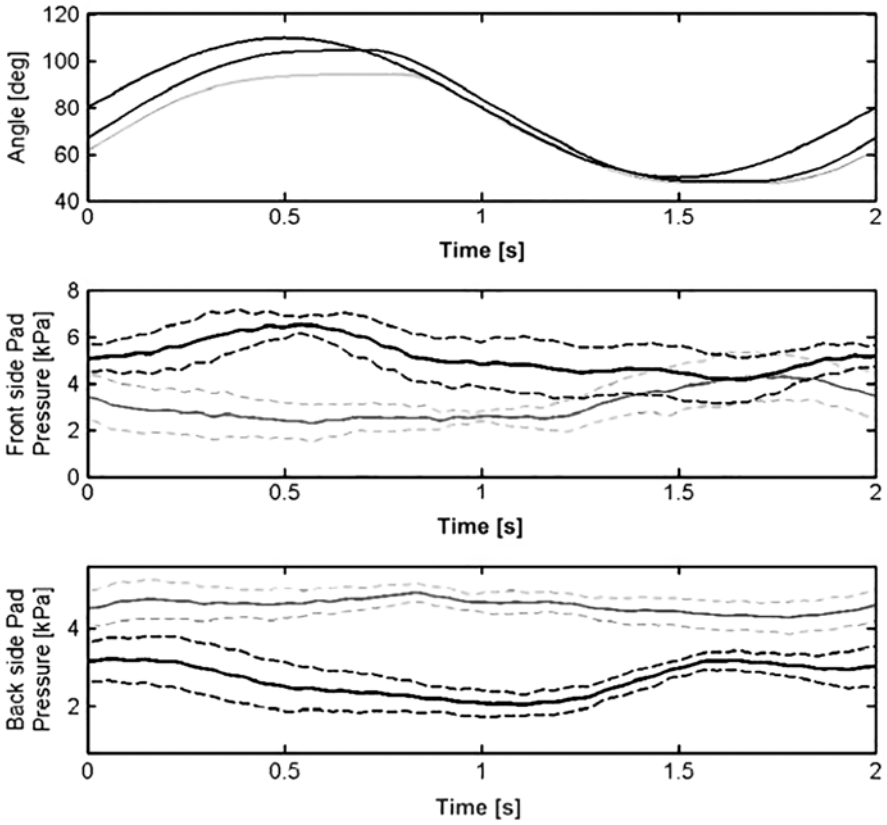


Fig. 7. Pressure profiles recorded during a prototypical rehabilitation task (represented on top by the elbow angle) on front- and backside of the forearm (black line represents no action of the user; gray line is with the user trying to faster the movement provided by the robot) © [2018] IEEE. Reprinted, with permission, from ref. [28].

exoskeleton.[27] Results showed that this passive mechanism resulted effective for unloading the joint from undesirable forces, while taking into account the inter-subject variability allowing rotations that are within the physiological displacements of the elbow axis during the movement ($\pm$ 5° and $\pm$ 3°, respectively).[26] In addition, the pressure profiles at the human–robot interface were measured in order to assess the usability and the comfort of the device.[28] A healthy volunteer had his elbow moved along flexion/extension trajectories in different loading conditions and the pressures on the back and on the front side of the forearm were measured. The results showed that, among all conditions, the pressure reached a maximum value in the central part of the pad around 7.5 kPa, well under the threshold of pain[29] (Fig. 7).

For the shoulder prototypes, the passive kinematic chain is designed to address mainly the shoulder protraction/retraction and elevation/depression, as well as the trunk rotations, in order to cover the workspace described by the shoulder centre of rotation within the exoskeleton workspace. In particular, the passive joints have been designed to guarantee translations along those directions higher than 10 cm when the exoskeleton is worn by the user, according to physiological data.[30,31] Figure 8a shows in detail how protraction/retraction and elevation/depression of the shoulder are allowed in NESM α. For NESM β (Fig. 8b), an additional horizontal translation movement (along the medio-lateral direction) is directly addressed by means of the mechanical connection between the exoskeleton and the support structure, to cover a higher "passive" workspace with respect to NESM α.

For future studies, a full characterization of the passive kinematic chains of both devices will be performed, similarly to the elbow prototype.

3.2. Compliance

The requirement of joint compliance has been addressed in all devices both via hardware (e.g. antagonistic remote actuation unit or SEAs) and via different software control strategies.

https://doi.org/10.1017/S0263574718001340 Published online by Cambridge University Press

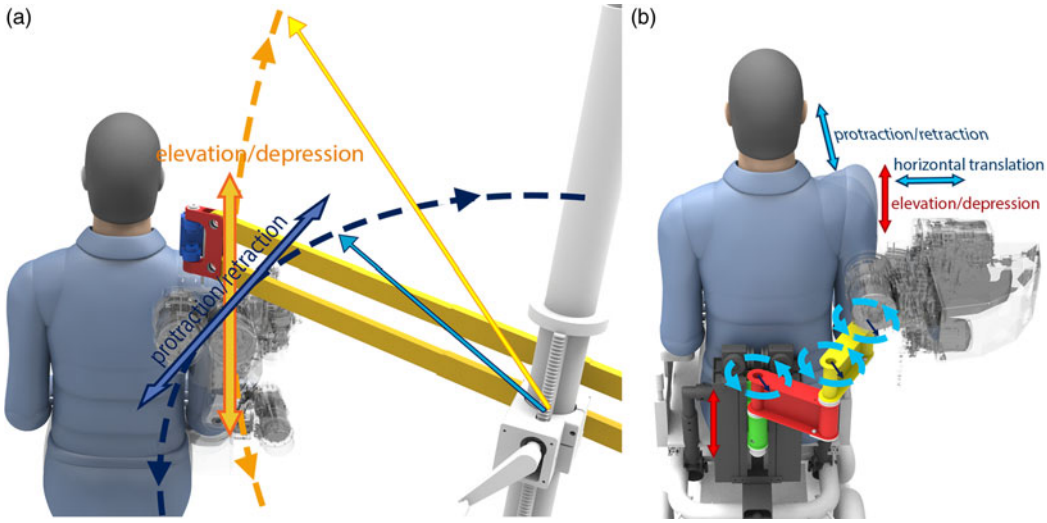


Fig. 8. Passive movements of the shoulder allowed by the passive DoFs chains of NESM α (a) and NESM β (b).

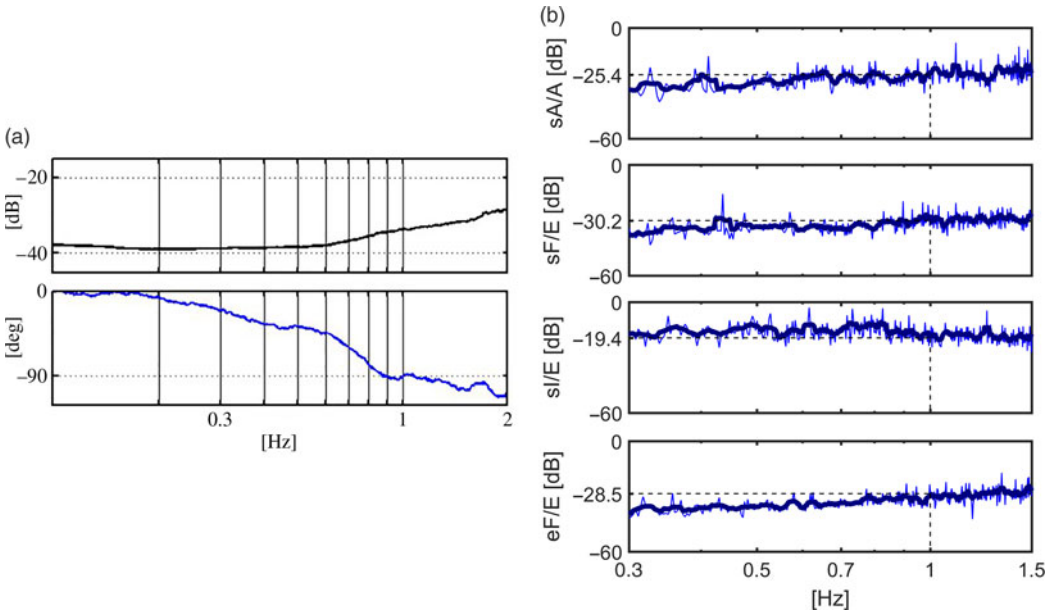


Fig. 9. Bode plots of the parasitic joint output impedance, normalized to the natural spring stiffness, for NEEM v2 (a) © [2018] IEEE. Reprinted, with permission, from ref. [32], and for NESM β (b).

On one hand, the actuation transparency has been assessed in the SEA prototypes by evaluating the joint output impedance when the devices are used in transparent mode. For this characterization, healthy users were requested to perform arm movements at different frequencies between 0.1 and 2 Hz, guided by a metronome, and the transfer function from the measured joint angle to the joint torque was calculated.

As shown in Fig. 9a, the NEEM v2 device resulted to be about 50 times more compliant than the spring natural stiffness (98.75 N·m/rad), with parasitic stiffness value of 1.97 N·m/rad for 1 Hz motion.[32] Similarly, for NESM β the parasitic stiffness at 1 Hz motion was 15.2, 9.3, 5.4, and 1.99 N·m/rad for sA/A, sF/E, sI/E, and eF/E, respectively (Fig. 9b). In the worst case, that is, for sI/E, the joint is about nine times more compliant than the spring natural stiffness.

For NEEM v1, the passive-compliance control performances were assessed by testing a prototypical rehabilitation task, in which a healthy volunteer undertook a 2-min session of passive mobilization along a sinusoidal trajectory: regulating the joint stiffness, the device attracted the human elbow

https://doi.org/10.1017/S0263574718001340 Published online by Cambridge University Press

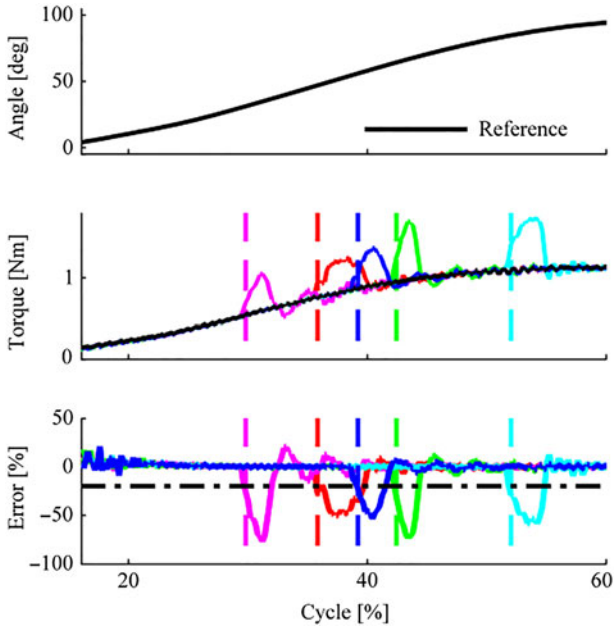


Fig. 10. Abnormal torque profiles detection algorithm. It operates on the difference between a reference torque profile and a perturbed one © [2018] IEEE. Reprinted, with permission, from ref. [25].

on the desired path with a mean square error decreasing from 12.1° to 4.96° with increasing stiffness. These results confirm that all the devices allow for a smooth human–robot interaction in their operative conditions.

In addition to transparency, a compliant behavior is paramount when the devices are used to treat people needing high-torque mobilization or exhibiting unpredictable arm movement (i.e. spasticity). This behavior was tested in NEEM v1 through the simulation of a spasmodic event: a healthy subject was asked to suddenly flex his arm as fast as possible and maintain the muscle contraction for few seconds during passive mobilization.[23] The maximum torque registered was around 8 N·m. Considering the studies present in literature, the elbow flexion and extension maximum torques are over 60 N·m,[33] meaning that the device, in case of sudden movements or resistance forces, prevents the spastic arm to be loaded with high and painful forces.

In the other prototypes where SEAs are employed, the accurate measurement of the joint torque allows the implementation of specific control strategies to deal with unpredictably joint movement. As an example, when NEEM v2 is used for passive mobilization of the elbow, a torque threshold can be set to a reasonable value according to the patient's level of impairment to deal with spasms by changing the control to *transparent mode* once the measured joint torque overcomes the threshold. An algorithm for the abnormal torque profiles detection (Fig. 10) was developed and evaluated on the elbow joint of NESM α.[25] First, the eF/E joint was moved in position control along a sigmoid trajectory for 20 times and the corresponding torque was recorded. The same test was repeated simulating a spastic contraction (touching the forearm cuff). The algorithm calculated the error between the reference torque profile (recorded in the first test) and the one recorded during the second test: every time that the torque was over 20% of the threshold, an abnormal torque profile was detected. Results from the offline analysis showed an average delay in detection lower than 50 ms for torque peaks between 0.5 and 2.5 N·m, demonstrating that this algorithm could be implemented in order to ensure safety in case of spasmodic events, typical of neurologic patients. An online version of the algorithm is currently under development.

3.3. Weight support

Although the elbow prototypes do not require a gravity compensation given the low weight of the moving parts (only the forearm double shell), a weight support is fundamental for the shoulder prototypes, in which the weight of the moving parts (i.e. the whole exoskeleton) is around 12 kg. For these prototypes, a feed-forward gravity compensation algorithm has been developed in order to ensure

https://doi.org/10.1017/S0263574718001340 Published online by Cambridge University Press

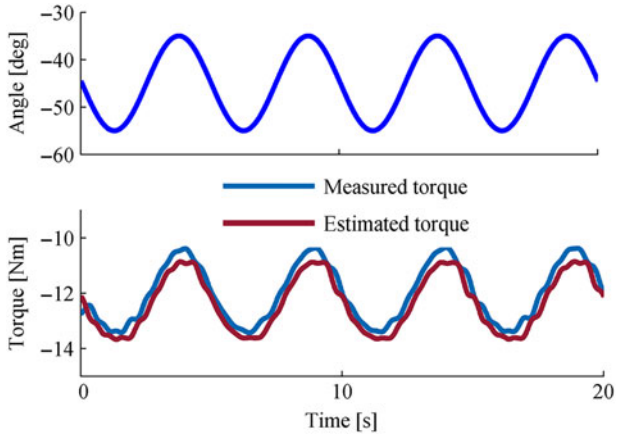


Fig. 11. Performance of the gravity compensation algorithm. Joint angle and measured versus estimated gravity torques for a representative joint (sA/A) during a dynamic trial © [2018] IEEE. Reprinted, with permission, from ref. [34].

that a specific amount of net torque is delivered to the joint, compensating for the torque due to gravity acting on it estimated as a function of the current exoskeleton pose.

An experimental session was conducted to validate the gravity compensation algorithm for NESM α, in both static and dynamic conditions.[34] The mean absolute error (MAE) between the desired torque calculated by the algorithm and the measured one was computed (Fig. 11), resulting to be lower than 0.3 N·m for eF/E and smaller than the values of the other joints (sA/A and sF/E), that in some cases reached up to 7 N·m. These outcomes could be related to the fact that the elbow is the last joint of the kinematic chain, and consequently the accuracy in identifying its center of mass and the link weight with respect to the other components of the exoskeleton is higher. These results showed good performance of the algorithm and demonstrated the effectiveness of the approach for implementing rehabilitative exercises that require a certain control of the provided torque. As of NESM β, the gravity compensation algorithm allows the flipping procedure while keeping the device on transparent mode, reducing the time and effort required to the external operator (e.g. the therapist) to change arm configuration.

3.4. Intention detection

Different control strategies and user's interfaces have been implemented and tested in all the devices, in order to detect effectively the user's intention to perform a certain action and provide adequate assistance to accomplish the movement.

The first study, on NEEM v1,[35] investigated the possibility to provide assistance using adaptive oscillators: these are designed to observe and predict the evolution of the variables of interest in a cyclical motion task, allowing to estimate in real time the phase of the cyclical movement, thus recognize the specific phase of the movement where the assistance is required. Each participant, with no experience with this protocol, was asked to cyclically move the elbow (with and without the exoskeleton) starting from a horizontal position, with a visual interface and a metronome to guide the movement pace. The surface EMG activity from the biceps brachii and triceps brachii muscles was recorded in order to monitor the participant's effort under different values of assistance. During the movements, the adaptive oscillator received as input the raw unfiltered position and estimated the angular position, velocity, and acceleration; the absolute error between these values and the measured ones was calculated in order to quantify the oscillator performance. In the trials without the exoskeleton, the position, velocity, and acceleration MAE were about 8.9%, 18.6%, and 32%, respectively. Providing assistance resulted in a progressive decreasing EMG peak value: the highest level of assistance showed a decrease of about 26% in the biceps peak and 59% in the triceps peak with respect to the movement without the exoskeleton. The oscillator resulted to filter the signal and predict its evolution introducing small delay, adapting to the users' behavior, in stationary conditions. At the same time, the users modulated the EMG activities according to the provided assistance; the kinematic profiles showed some transient effects in the estimation due to the change of the assistive modes. This "double-direction adaptation" (from the oscillator to the user and from the user to the

https://doi.org/10.1017/S0263574718001340 Published online by Cambridge University Press

provided assistance) highlights the advantages of using adaptive oscillator for providing assistance to observe and predict cyclical movements.

On NESM α, an experimental session has been conducted on to evaluate the usability and the effectiveness of EMG interfaces to detect the user's intention to initiate the movement.[36] During the test, a healthy subject wearing the exoskeleton was seated in front of a screen with three LEDs (placed on the left, center, and right), which were switched on in a random order. The user was requested to move toward the LED turned on, with the robot in *transparent mode*. The signals from seven arm muscles and the kinematic variables from the exoskeleton were recorded and analyzed offline. The EMG signals were used to segment the reaching task in rest and movement phases by extracting a set of four features from three different sources: a single EMG signal, multiple EMG signals in parallel, and a compound EMG signal, including the contribution of all the recorded muscles as a single signal. Then, alone and in combination with kinematics data, these features were used to realize a classifier able to identify the user's intention in terms of movement onset time and direction. The 70% of the available data was used to train this classification algorithm and the remaining 30% for testing. The compound EMG signal method resulted to detect movement onset much earlier than the other two, about 40 ms before the reference onset time. Correct classification of movement direction was 61% on average when the features of the EMG signals alone were used as inputs for the classifier; performance increased to 89% by adding the kinematic information from the exoskeleton. This algorithm showed a good performance in detecting user's motion intention suggesting potential future implementation in the control of the device for more custom therapy.

In ref. [37], a shared human–machine control system, designed to perform ADLs and integrating the NESM α, a wrist–hand exoskeleton, and a hybrid electroencephalography/electrooculography (EEG/EOG) interface, was tested on seven healthy subjects. The control system, implemented on the NESM α, was based on a finite-state machine where the main task was split into different sub-actions, in which execution or interruption was controlled by the user by means of the EEG/EOG interface. Feasibility and safety of the shared control paradigm was demonstrated, opening the way to further clinical testing in the context of neurorehabilitation or assistance in daily-life scenarios. For the latter, the possibility to integrate the NESM β into an electric wheelchair represents a promising solution to bring such control paradigm in everyday life environment.

3.5. Clinical studies

After the characterization of the devices by tests on healthy subjects, the final goal is to evaluate on which extent these design requirements are translated into the clinical practice.

For this purpose, a phase-II clinical validation study was conducted at the Auxilium Vitae Rehabilitation Centre of Volterra (Pisa, Italy) to assess the NEEM v2 safety and efficacy in the treatment of elbow spasticity. A group of 17 post-stroke patients in their sub-acute phase underwent a robotic rehabilitation treatment, consisting of isokinetic passive mobilization, executed for 10 consecutive working days, in addition to traditional physical therapy. Each session consisted of 45 min of elbow flexion/extension (90 cycles) at a constant velocity of 20°/s with the device set in position control. The physical therapist assessed the ROM, Chedoke-McMaster Stroke Assessment Measure (CMSA), and the Modified Ashwort Scale (MAS) at the beginning and at the end of the treatment; a follow-up assessment was conducted 3 months after the stroke. From the kinematic variables recorded from the sensing apparatus, considering only the extension phase (all the participants had spasticity on the elbow flexors), the torque exerted at the maximum extension angle (MET) and the angle correspondent to a null exerted torque (ZTA) were extracted as indicators of the resistance to the movement.[38] The absence of mechanical or electrical failures, damages to the device, or undesired effects on the patients during the entire duration of the treatment demonstrated the safety of the device for treating patients with different body sizes and motor impairments for long periods. This behavior suggested that a treatment program provided with this device in the early post-stroke phase could contribute to the spasticity prevention. Moreover, the correlation between the extracted parameters and the score of the traditional clinical assessment scale suggests the potential use of the device not only for the treatment but also for the quantitative evaluation of motor recovery. Nevertheless, the relatively small group of patients of the study and the absence of a control group did not allow to reach conclusions applicable to larger populations. Future works will be focused on the design of controlled studies with a larger number of patients, extending this approach to the shoulder prototypes as well.

https://doi.org/10.1017/S0263574718001340 Published online by Cambridge University Press

Table I. Main design characteristics of the upper-limb exoskeletons developed at Scuola Superiore Sant'Anna.

	Passive DOFs	Active DOFs		Control modalities		Max torque [N·m]	Spring stiffness [N·m/rad]	Range of motion [°]
NEEM v1.0	4	1	eF/E	Passive compliance	Torque–Force	15	–	0°:130°
NEEM v2.0	4	1	eF/E	Position	Torque	30	98	0°:130°
NESM α	8	4	sA/A	Position	Torque	60	166	−90°:0°
			sF/E	Position	Torque	60	166	−90°:0°
			sI/E	Position	Torque	30	92	−80°:25°
			eF/E	Position	Torque	30	92	0°:125
NESM β	5	4	sA/A	Position	Torque	35	280	−85°:0°
			sF/E	Position	Torque	35	300	−85°:0°
			sI/E	Position	Torque	15	50	−90°:30°
			eF/E	Position	Torque	15	50	0°:90°

4. Conclusions

In this paper, we have presented a novel generation of upper-limb robotic exoskeletons for neurologic rehabilitation developed at Scuola Superiore Sant'Anna. The latest version of the upper-limb exoskeleton, NESM β, is presented here for the first time. For direct comparison, Table I summarizes the main design characteristics of the four devices presented herein.

The presented devices have been designed to satisfy the main requirements of a human–robot interface for a wearable robot to provide rehabilitation and assistance. Each prototype fulfils the requirements with different approaches developed over time. The physical compliance, needed for providing a smooth and safe interface able to manage sudden and resistive movements typical in subjects affected by spasticity, is obtained by a combination of mechanical design and active control. The first prototype (NEEM) is composed of a pair of remote and independent antagonistic actuation units that can regulate the stiffness of the joint through a dedicated control strategy, while the three subsequent devices implement a series elastic actuation (SEA) architecture to ensure a smooth interaction with the user. As a measure of the actuation transparency of the devices, the parasitic joint output impedances of the NEEM and NESM β in transparent mode have been computed, and results in both cases guarantee a comfortable human–robot interaction in zero-torque control mode, despite their different levels of mechanical complexity.

The joint axis self-alignment is guaranteed in the two versions of NEEM by the same 4-DoF passive mechanism that unloads the elbow joint from undesired forces, while in the NESM shoulder–elbow devices, the overall structure includes additional passive DoFs in order to comply with the complex motion of the whole shoulder girdle. Conversely, the 4-DoF self-aligning mechanism for the NESM elbow has been simplified to a single passive DoF movement.

The whole-arm wearable exoskeletons have been designed to follow the main movements of shoulder and elbow joints, as shown in Fig. 8. Although experiments with passive degrees of freedom locked have not been conducted, the control algorithms and the mechanical properties have been designed and demonstrated to reliably prevent the user from experiencing undesired and potentially painful or injurious loads. In this way, the NEEM and NESM software and hardware designs (i.e. torque safety thresholds and intrinsic compliance of the SEA units) combine to make the devices safe for users.

Moreover, the wearability and comfort of all NeuroExos devices have been improved by the ergonomic pHRI structures that conform to the upper arm and the forearm, composed of a thermo-formed double-shell structure, with inner shell covered by soft material.

The possibility to treat both the right and left arms with the recent NESM β prototype and to mount it directly on a wheelchair extends its potential field of application with respect to the previous devices.

The possibility of controlling individual joint torques allows exoskeletal robots to assist or resist the articulation of individual joints, as needed in rehabilitative treatments. As an example, in ref. [39], a patient involved in an object manipulation task executed with an exoskeleton controlled in force modality and weight compensation showed the adoption of compensation strategies for the

https://doi.org/10.1017/S0263574718001340 Published online by Cambridge University Press

adduction–abduction forearm motion via the shoulder girdle. On the other hand, controlling specific joints allows highly customized rehabilitation programs, according to each patient's specific movement capabilities, that is, adapting the exercises throughout all phases of recovery, by tuning maximum torque values depending on subjects' specific thresholds for activation of stretch reflexes.[6]

In the NEUROExos design evolution, particular effort has been devoted to improve existing features or adding new ones while reducing the overall complexity of the system. As shown in Fig. 6b, the NESM β, with its support structure (i.e. the wheelchair), has an overall encumbrance comparable to the elbow prototype, despite having a higher number of active and passive DoFs in the kinematic chain and, at the same time, satisfying the requirement of portability outside clinical settings.

In all experimental studies, the NEUROExos devices exhibited clinically relevant performance in terms of reliability, safety, and effectiveness, thus laying the foundation for future development and clinical validation studies. The robotic system performances in delivering patient-in-charge and robot-in-charge movement assistance suggest the possibility of delivering therapy personalized for each patient able to adapt to the different phases of the recovery. The gravity compensation feature becomes essential especially for multiple DoF movements, hence for the shoulder–elbow devices, and has shown to be effective for implementing rehabilitative exercises that demand specific control of the torque value. Different approaches for treating patients able to participate in the movement, that is, the use of adaptive oscillators or the EMG-based intention detection, seem promising for providing assistance and warrant further investigations. Many studies indeed have shown that intensive, repetitive, task-specific training can significantly improve motor functions in chronic stroke patients even years after stroke, resulting in one of the most effective approaches to restore the arm function.[40,41] Considering that the use of adaptive oscillators for providing assistance is investigated for observing and predicting cyclical movement,[35] this method could be promising in performing stereotyped rehabilitative tasks for the shoulder–elbow complex as well. Future studies will be conducted in order to investigate this possibility.

As for the EMG-based intention detection, the proposed method was mainly focused on the detection of movement intention and direction, rather than a direct control of the exoskeleton through EMG signals. In the case of post-stroke subjects, taking into consideration that during reaching tasks multiple muscles are involved in the movement, the abnormal muscle tone can make arduous the identification of a group of them to appropriately tune the control of the robot. In this case, the method can be applied to trigger the execution of an "assist as needed" functional task by detecting the onset of muscular activity from a single selected muscle or small combination of muscles.

Future studies will also address the possibility to deliver assistance in ADL in a home environment, to provide functional rehabilitation, and to develop standardized methods for clinical assessment.

Acknowledgments

Authors would like to acknowledge Eng. Filippo Dell'Agnello for the technical support in the development of the electronics and fellow researcher Zach McKinney for his role in proofing and editing the final manuscript copy.

Conflict of Interest

A. Baldoni, S. Crea, and N. Vitiello have commercial interests in IUVO S.r.l., a spinoff company of Scuola Superiore Sant'Anna. Currently, part of the IP protecting the NEEM, NESM α, and NESM β technology described in the paper has been licensed to IUVO S.r.l. for commercial exploitation.

Funding Statement

This work was supported in part by the Regione Toscana within the RONDA Project (Bando FAS Salute 2014) and in part by the European Union within the AIDE Project H2020-ICT-22-2014 under Grant Agreement 645322.

References

1. P. Poli, G. Morone, G. Rosati and S. Masiero, "Robotic technologies and rehabilitation: New tools for stroke patients," *Biomed. Res. Int.* **2013**, Art. ID 153872 (2013).
2. B. T. Volpe, D. Lynch, A. Rykman-Berland, M. Ferraro, M. Galgano, N. Hogan and H. I. Krebs, "Intensive sensorimotor arm training mediated by therapist or robot improves hemiparesis in patients with chronic stroke," *Neurorehabil. Neural Repair* **22**(3), 305–310 (2008).

https://doi.org/10.1017/S0263574718001340 Published online by Cambridge University Press

3. P. S. Lum, C. G. Burgar, P. C. Shor, M. Majmundar and M. Van der Loos, "Robot-assisted movement training compared with conventional therapy techniques for the rehabilitation of upper-limb motor function after stroke," *Arch. Phys. Med. Rehabil.* **83**(7), 952–959 (2002).
4. N. Hogan, H. I. Krebs, J. Charnnarong, P. Srikrishna and A. Sharon, "MIT-MANUS: A workstation for manual therapy and training. I," *Proceedings, IEEE International Workshop on Robot and Human Communication, 1992*, Tokyo, Japan (1992) pp. 161–165.
5. S. Coote, B. Murphy, W. Harwin and E. Stokes, "The effect of the GENTLE/s robot-mediated therapy system on arm function after stroke," *Clin. Rehabil.* **22**(5), 395–405 (2008).
6. P. S. Lum, C. G. Burgar, D. E. Kenney and M. Van der Loos, "Quantification of force abnormalities during passive and active-assisted upper-limb reaching movements in post-stroke hemiparesis," *IEEE Trans. Biomed. Eng.* **46**(6), 652–662 (1999).
7. J. C. Perry, J. Rosen and S. Burns, "Upper-limb powered exoskeleton design," *IEEE/ASME Trans. Mechatron.* **12**(4), 408–417 (2007).
8. A. H. A. Stienen, E. E. G. Hekman, F. C. T. Van der Helm and H. Van der Kooij, "Self-aligning exoskeleton axes through decoupling of joint rotations and translations," *IEEE Trans. Robot.* **25**(3), 628–633 (2009).
9. T. Proietti, V. Crocher, A. Roby-Brami and N. Jarrasse, "Upper-limb robotic exoskeletons for neurorehabilitation: A review on control strategies," *IEEE Rev. Biomed. Eng.* **9**, 4–14, (2016).
10. S. J. Ball, I. E. Brown and S. H. Scott, "MEDARM: A rehabilitation robot with 5DOF at the shoulder complex," *2007 IEEE/ASME International Conference on Advanced Intelligent Mechatronics*, Zurich, Switzerland (2007) pp. 1–6.
11. X. Cui, W. Chen, X. Jin and S. K. Agrawal, "Design of a 7-DOF cable-driven arm exoskeleton (CAREX-7) and a controller for dexterous motion training or assistance," *IEEE/ASME Trans. Mechatron*. **22**(1), 161–172 (2016).
12. A. Otten, H. C. Voort, A. H. A. Stienen, R. G. K. M. Aarts, E. H. F. Van Asseldonk and H. Van der Kooij, "Limpact: A hydraulically powered self-aligning upper limb exoskeleton," *IEEE/ASME Trans. Mechatron*. **20**(5), 2285–2298 (2015).
13. A. H. A. Stienen, E. E. G. Hekman, F. C. T. Van der Helm, G. B. Prange, M. J. A. Jannink, A. M. M. Aalsma and H. Van der Kooij, "Dampace: Dynamic force-coordination trainer for the upper extremities," *IEEE 10th International Conference on Rehabilitation Robotics, 2007*, Noordwijk, Netherlands (2007) pp. 820–826.
14. B. Kim and A. D. Deshpande, "An upper-body rehabilitation exoskeleton Harmony with an anatomical shoulder mechanism: Design, modeling, control, and performance evaluation," *Int. J. Rob. Res*. **36**(4), 414–435 (2017).
15. E. Pirondini, M. Coscia, S. Marcheschi, G. Roas, F. Salsedo, A. Frisoli, M. Bergamasco and S. Micera, "Evaluation of the effects of the Arm Light Exoskeleton on movement execution and muscle activities: A pilot study on healthy subjects," *J. Neuroeng. Rehabil*. **13**(1), 9 (2016).
16. J. Heinzmann and A. Zelinsky, "Quantitative safety guarantees for physical human-robot interaction," *Int. J. Rob. Res*. **22**(7–8), 479–504 (2003).
17. G. A. Pratt and M. M. Williamson, "Series elastic actuators," *1995 IEEE/RSJ International Conference on Intelligent Robots and Systems 95 "Human Robot Interaction and Cooperative Robots" Proceedings*, Pittsburgh, PA (1995) pp. 399–406.
18. R. Morales, F. J. Badesa, N. Garcia-Aracil, J. M. Sabater and C. Perez-Vidal, "Pneumatic robotic systems for upper limb rehabilitation," *Med. Biol. Eng. Comput*. **49**(10), 1145–1156 (2011).
19. R. J. Sanchez, E. Wolbrecht, R. Smith, J. Liu, S. Rao, S. Cramer, T. Rahman, J. E. Bobrow and D. J. Reinkensmeyer, "A pneumatic robot for re-training arm movement after stroke: Rationale and mechanical design," *IEEE 9th International Conference on Rehabilitation Robotics, Proceedings of the 2005*, Chicago, IL (2005) pp. 500–504.
20. T. G. Sugar, J. He, E. J. Koeneman, J. B. Koeneman, R. Herman, H. Huang, R. S. Schultz, D. E. Herring, J. Wanberg, S. Balasubramanian, P. Swensons and J. A. Ward, "Design and control of RUPERT: A device for robotic upper extremity repetitive therapy," *IEEE Trans. Neural. Syst. Rehabil. Eng.* **15**(3), 336–346 (2007).
21. C. T. O'Neill, N. S. Phipps, L. Cappello, S. Paganoni and C. J. Walsh, "A soft wearable robot for the shoulder: Design, characterization, and preliminary testing," *2017 International Conference on Rehabilitation Robotics*, London, UK (2017) pp. 1672–1678.
22. M. Xiloyannis, L. Cappello, K. D. Binh, C. W. Antuvan and L. Masia, "Preliminary design and control of a soft exosuit for assisting elbow movements and hand grasping in activities of daily living," *J. Rehabil. Assist. Technol. Eng.* **4**, 1–15 (2017).
23. T. Lenzi, N. Vitiello, S. M. M. De Rossi, S. Roccella, F. Vecchi and M. C. Carrozza, "NEUROExos: A variable impedance powered elbow exoskeleton," *2011 IEEE International Conference on Robotics and Automation (ICRA)*, Shanghai, China (2011) pp. 1419–1426.
24. M. Cempini, F. Giovacchini, N. Vitiello, M. Cortese, M. Moisé, F. Posteraro and M. C. Carrozza, "NEUROExos: A powered elbow orthosis for post-stroke early neurorehabilitation," *2013 35th Annual International Conference of the IEEE Engineering in Medicine and Biology Society (EMBC)*, Osaka, Japan (2013) pp. 342–345.
25. S. Crea, M. Cempini, M. Moisé, A. Baldoni, E. Trigili, D. Marconi, M. Cortese, F. Giovacchini, F. Posteraro and N. Vitiello, "A novel shoulder-elbow exoskeleton with series elastic actuators," *2016 6th IEEE International Conference on Biomedical Robotics and Biomechatronics (BioRob)*, Singapore, Singapore (2016) pp. 1248–1253.

https://doi.org/10.1017/S0263574718001340 Published online by Cambridge University Press

26. M. Bottlang, S. M. Madey, C. M. Steyers, J. L. Marsh and T. D. Brown, "Assessment of elbow joint kinematics in passive motion by electromagnetic motion tracking," *J. Orthop. Res.* **18**(2), 195–202 (2000).
27. N. Vitiello, T. Lenzi, S. Roccella, S. M. M. De Rossi, E. Cattin, F. Giovacchini, F. Vecchi and M. C. Carrozza, "NEUROExos: A powered elbow exoskeleton for physical rehabilitation," *IEEE Trans. Robot.* **29**(1), 220–235 (2013).
28. T. Lenzi, N. Vitiello, S. M. M. De Rossi, A. Persichetti, F. Giovacchini, S. Roccella, S. Vecchi and M. C. Carrozza, "Measuring human-robot interaction on wearable robots: A distributed approach," *Mechatronics* **21**(6), 1123–1131 (2011).
29. C. Calvo Lobo, C. Romero Morales, D. Rodríguez Sanz, I. Sanz Corbalán, E. A. Sánchez Romero, J. Fernández Carnero and D. López López, "Comparison of hand grip strength and upper limb pressure pain threshold between older adults with or without non-specific shoulder pain," *Peer J.* 5, e2995 (2017).
30. D. T. Harryman, J. A. Sidles, J. M. Clark, K. J. McQuade, T. D. Gibb and F. A. Matsen, "Translation of the humeral head on the glenoid with passive glenohumeral motion," *J. Bone Joint Surg. Am.* **72**(9), 1334–1343 (1990).
31. T. Nef and R. Riener, "Shoulder actuation mechanism for arm rehabilitation," *2nd IEEE RAS & EMBS International Conference on Biomedical Robotics and Biomechatronics,* Scottsdale, AZ (2008).
32. N. Vitiello, M. Cempini, S. Crea, F. Giovacchini, M. Cortese, M. Moisé, F. Posteraro and M. C. Carrozza, "Functional design of a powered elbow orthosis toward its clinical employment," *IEEE/ASME Trans. Mechatron.* **21**(4), 1880–1891 (2016).
33. F. Guenzkofer, H. Bubb and K. Bengler, "Maximum elbow joint torques for digital human models," *Int. J. Human Factors Modell. Sim.* **3**(2), 109–132 (2012).
34. S. Crea, M. Cempini, M. Moisé, A. Baldoni, E. Trigili, D. Marconi, M. Cortese, F. Giovacchini, F. Posteraro and N. Vitiello, "Validation of a Gravity Compensation Algorithm for a Shoulder-Elbow Exoskeleton for Neurological Rehabilitation," **In**: *Converging Clinical and Engineering Research on Neurorehabilitation II* (Springer International Publishing, Cham, 2016) pp. 495–499.
35. R. Ronnse, N. Vitiello, T. Lenzi, J. Van den Kieboom, M. C. Carrozza and A. J. Ijspeert, "Human-robot synchrony: Flexible assistance using adaptive oscillators," *IEEE Trans. Biomed. Eng.* **58**(4), 1001–1012 (2011).
36. A. Accogli, L. Grazi, S. Crea, A. Panarese, J. Carpaneto, N. Vitiello and S. Micera, "EMG-based Detection of User's Intentions for Human-Machine Shared Control of an Assistive Upper-Limb Exoskeleton," **In**: *Wearable Robotics: Challenges and Trends* (Springer International Publishing, Cham, 2016) pp. 181–185.
37. S. Crea, M. Nann, E. Trigili, F. Cordella, A. Baldoni, F. J. Badesa, J. M. Catalan, L. Zollo, N. Vitiello, N. G. Aracil and S. R. Soekadar, "Feasibility and safety of shared EEG/EOG and vision-guided autonomous whole-arm exoskeleton control to perform activities of daily living," *Sci. Rep*. **8**(1), 10823 (2018).
38. S. Crea, M. Cempini, S. Mazzoleni, M. C. Carrozza, F. Posteraro and N. Vitiello, "Phase-II clinical validation of a powered exoskeleton for the treatment of elbow spasticity," *Front. Neurosci.* **11**, 261–270 (2017).
39. A. Frisoli, L. Borelli, A. Montagner, S. Marcheschi, C. Procopio, F. Salsedo, M. Bergamasco, M. C. Carboncini, M. Tolaini and B. Rossi, "Arm rehabilitation with a robotic exoskeleton in Virtual Reality," *IEEE 10th International Conference on Rehabilitation Robotics, 2007*, Noordwijk, Netherlands (2007) pp. 631–642.
40. P. Staubli, T. Nef, V. Klamroth-Marganska and R. Riener, "Effects of intensive arm training with the rehabilitation robot ARMin II in chronic stroke patients: Four single-cases," *J. Neuroeng. Rehabil*. **6**(1), 46 (2009).
41. S. Barreca, S. L. Wolf, S. Fasoli and R. Bohannon, "Treatment interventions for the paretic upper limb of stroke survivors: A critical review," *Neurorehabil. Neural Repair* **17**(4), 220–226 (2004).

https://doi.org/10.1017/S0263574718001340 Published online by Cambridge University Press